Toward Molecular Nanowires Self-Assembled on an Insulating Substrate: Heptahelicene-2-carboxylic acid on Calcite ($10\bar{1}4$)

Philipp Rahe,[†,§] Markus Nimmrich,[†,§] Andreas Greuling,[†] Jens Schütte,[†] Irena G. Stará,*[,‡] Jiří Rybáček,[‡] Gloria Huerta-Angeles,[‡] Ivo Starý,[‡] Michael Rohlfing,[†] and Angelika Kühnle*[,†,§]

Fachbereich Physik, Universität Osnabrück, Barbarastraβe 7, 49076 Osnabrück Germany, and Institute of Organic Chemistry and Biochemistry, Academy of Sciences of the Czech Republic, v. v. i., Flemingovo nám. 2, 166 10 Prague 6, Czech Republic

Received: November 27, 2009

Molecular self-assembly is employed for creating unidirectional molecular nanostructures on a truly insulating substrate, namely the ($10\bar{1}4$) cleavage plane of calcite. The molecule used is racemic heptahelicene-2-carboxylic acid, which forms structures, well-aligned along the [010] crystallographic direction and stable at room temperature. Precise control of both molecule−substrate and molecule−molecule interaction is required, leading to the formation of such wire-like structures of well-defined width and lengths exceeding 100 nm. This subtle balance is governed by the heptahelicene-2-carboxylic acid used in this study, allowing for both hydrogen bond formation as well as $\pi-\pi$ stacking.

Introduction

Fabricating electronic devices at the molecular scale is a promising strategy to overcome the physical limitations arising from further miniaturization of state-of-the-art silicon technology.[1] Building devices on the scale of single molecules provides the potential of improved efficiency, higher computational speed, and cost-effective production.[2] Two elementary structures are pivotal for the fabrication of future molecular electronic devices, namely molecular transistors[3] and wires in form of quasi one-dimensional arrangements.[4] Several concepts for single-molecule transistors have already been developed,[3] and their switching capability has been demonstrated.[5]

For bottom-up fabrication of molecular structures, the promising concept of self-assembly has attracted great attention.[6,7] Especially on conducting and semiconducting surfaces, a large variety of structures ranging from quasi zero-dimensional structures[8] to complex network structures[9,10] has been presented. In contrast, only little progress has been made so far on insulating substrates, although future molecular electronic applications will require nonconducting substrates. Very recently, the first promising results have been obtained on a truly insulating substrate, namely KBr(001).[4,11–13] In these studies, an attempt has been made to form molecular wire-like structures, however, high molecular mobility has led to clustering at the step edges[4,14] or the formation of structures of several tens of nanometers in width.[15] It has been demonstrated that the length can be controlled by employing Au nanoclusters as end-caps, however, both width and height of these molecular structures have remained less well controlled.[11,12]

Herein, we present the formation of unidirectional molecular structures self-assembled from heptahelicene-2-carboxylic acid ([7]HCA). In contrast to the previous results on insulating surfaces, the wire-like structures observed here grow on bare terraces and are of well-defined width. We use racemic [7]HCA (enantiomeric excess of 0%), an equimolar mixture of (*M*)-[7]HCA and (*P*)-[7]HCA differing in helicity as depicted in Figure 1a.

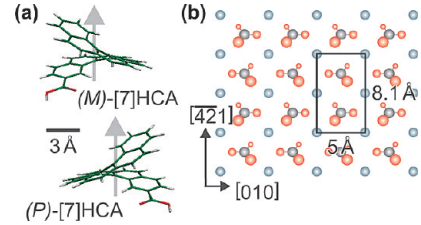

Figure 1. (a) Model of the [7]HCA molecule. The molecule is functionalized by a carboxylic group attached to one end of the screw structure. The helical molecular axis is marked by a gray arrow. In this study, the racemic mixture (enantiomeric excess of 0%) of both enantiomers was used. (b) The calcite ($10\bar{1}4$) surface possesses a rectangular surface unit cell with dimensions of 5 Å × 8.1 Å. Two alternating carbonate groups rotated relative to the surface normal are located within the unit cell.

The [7]HCA molecule was functionalized with a carboxylic acid moiety, influencing the intermolecular interaction and eventually the molecular order. The π-system, on the other hand, provides the potential for electric transport along several molecules. The transport along single helicene molecules has been studied theoretically,[16] demonstrating that by tuning the radius of the helix and the width of the helix ribbon, helicenes exhibit semiconducting or metallic behavior. Bare heptahelicenes ([7]H) without a carboxylic acid moiety have been investigated before on different metal surfaces, namely Cu(111),[17–19] Cu(332),[18] Ni(100)[20] and Ni(111).[21] On the Cu surfaces, [7]H molecules bind via the three terminal phenyl rings to the substrate, with its helical axis nearly parallel to the surface normal.[18,19] On Ni(100), by contrast, [7]H molecules within a saturated monolayer adsorb with their helical axis at an angle of 43 ± 5° with respect to the surface plane.[20] This geometry, identified by NEXAFS for Ni(100), is suggested but not confirmed for a closed monolayer on Ni(111).[21]

* To whom correspondence should be addressed. Phone: ++49 6131 39 23930. E-mail: kuehnle@uni-mainz.de (A.K.); stara@uochb.cas.cz (I.G.S.).
† Universität Osnabrück.
‡ Academy of Sciences of the Czech Republic.
§ Present address: Institut für Physikalische Chemie, Johannes Gutenberg-Universität Mainz, Jakob-Welder-Weg 11, 55099 Mainz, Germany.

10.1021/jp911287p
Published on Web 12/28/2009

The underlying substrate in this study is the $(10\bar{1}4)$ cleavage plane of calcite, the most stable polymorph of calcium carbonate. As depicted in Figure 1b, the surface unit cell is rectangular with dimensions of 5.0 Å × 8.1 Å. The carbonate groups, two of which are located inside one unit cell, are rotated with respect to the surface normal and with respect to each other. This leads to a zigzag structure of the topmost oxygen atoms along the [-4-21] direction.

The $(10\bar{1}4)$ surface of calcite has been studied intensively under aqueous conditions because of its significant impact in many areas of both fundamental research and applied science ranging from biomineralization[22] through growth properties under molecular influences[23] to its abundant occurrence in natural oil resources.[24] Using noncontact atomic force microscopy (NC-AFM), which has been proven to be an indispensable tool for studying nonconducting surfaces with the highest precision,[25] direct imaging of the calcite $(10\bar{1}4)$ surface under ultrahigh vacuum (UHV) conditions is possible down to the atomic level, including the identification of single surface defects.[26]

Methods

The calcite $(10\bar{1}4)$ surfaces were prepared in-vacuo by cleavage of a bulk crystal.[27] The crystals were of highest available quality from Korth Kristalle GmbH. Prior to cleavage, the crystals were degassed to 550 K for removing contaminants near the sample. After cleavage, the crystals were annealed for 1.5 h to 550 K to remove surface charges. The racemic [7]HCA was prepared from known [7]Helicen-2-ol,[28] whose synthesis relied on the triyne [2 + 2 + 2] cycloisomerization methodology we had developed earlier.[29–32] Experimental procedures will be published separately as a part of a broader study on the synthesis of functionalized [7]Helicenes. It was characterized by spectroscopic methods (^{1}H and ^{13}C NMR, ESI and APCI MS). The [7]HCA sample was filled into a glass crucible with a thermocouple melted into the closed end and a filament wrapped around it. The sublimation temperature was identified by depositing molecules with the temperature of the crucible successively increasing.

All experiments were carried out in a UHV system with a base pressure below 10^{-10} mbar, as described previously.[33] The NC-AFM experiments were performed with an Omicron (Taunusstein, Germany) VT AFM 25. The microscope was operated in the frequency modulated noncontact mode using an easyPLL Plus from Nanosurf (Liestal, Switzerland) for oscillation excitation and signal demodulation.[25,34] We used doped silicon cantilevers of the PPP-NCH type from Nanosensors (Neuchâtel, Switzerland), which were sputtered by Ar^+ once after introduction into the UHV system. All of the presented images are raw data except for a plane subtraction applied to all of the topography data. The time needed for recording one image accounts to approximately 8.5 min.

The density functional theory (DFT) calculations presented here were conducted in the local density approximation (LDA) with a Ceperley Alder exchange correlation potential.[35] We applied the SIESTA code[36,37] using a mesh cutoff of 130 Ry and a double-zeta polarized basis set.[37] The core electrons are replaced by nonlocal norm-conserving Troullier-Martins pseudopotentials.[38] The pseudopotentials we used were generated by means of the atom program, which comes with the SIESTA package. For carbon and oxygen, we considered 2s and 2p orbitals, while 1s was placed in the frozen core. The cutoff radii for oxygen were 1.15 Bohr (2s and 2p) and 1.25 Bohr (2s and 2p) for carbon. The binding energies given were corrected for the basis set superposition error (BSSE) using the so-called counterpoise (CP)/ghost orbital approach.[39,40]

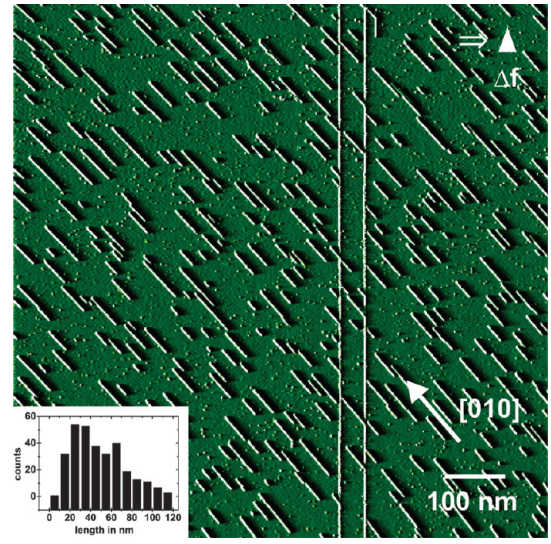

Figure 2. Detuning image of the calcite $(10\bar{1}4)$ surface including the adsorbed molecules taken approximately 6 h after finishing the molecule deposition. Two step edges of the underlying substrate are visible as vertical, straight lines. Unidirectional molecular rows are observed along the [010] direction. The length distribution of these rows is presented in the inset.

Results and Discussion

The [7]HCA molecules were sublimated onto the bare calcite surface kept at room temperature from a heated crucible. Figure 2 displays an overview image taken approximately 6 h after depositing the molecules. Within this image, single rows located on the calcite surface are clearly visible. All of the rows are aligned along the [010] direction. The mean length of the rows in this image is 47 nm with a standard deviation of 24 nm, reflecting the length distribution of the molecular rows as presented in the inset of Figure 2. In contrast, the width of the rows is monodisperse and will be discussed later. The distribution of the rows on the surface is random apart from the alignment along the [010] direction. At room temperature, we never observed straight rows along another crystallographic direction. Furthermore, neither clustering nor island formation of the molecular rows was observed at this coverage of about one-quarter of a full monolayer.[41] Additionally, there is no indication of nucleation at the step edges of the calcite substrate. Two step edges are observed in Figure 2 as straight lines running through the entire image from top to bottom. As can be seen, the edges do not constitute nucleation sites for the growth of molecular rows.

The molecular rows shown here form at room temperature and do not require further treatment such as annealing at elevated temperatures. In the early stages of row formation, we do, however, observe a transient row structure, having a smaller width than the final molecular rows. Such transient rows can be seen in Figure 3, taken ~65 min after molecule sublimation. In this image, two different molecular row structures coexist, namely the molecular rows as identified in Figure 2 and, additionally, thinner rows which have approximately half of the previously observed width (a few of these thinner rows are marked by arrows). This observation together with the distances identified later indicate that the final molecular row structures are composed of molecular pairs.

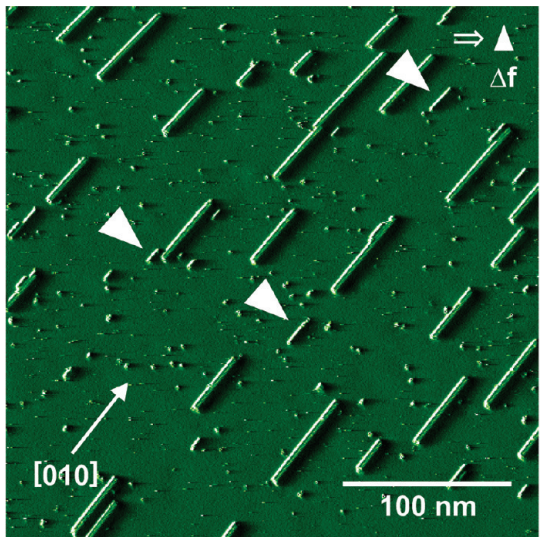

Figure 3. Detailed view of the unidirectional molecular structures. In contrast to Figure 2, this image was started ~65 min after the molecule deposition was finished. Distinct rows of two different widths are present; the broader rows resemble the rows observed in Figure 2. Several thinner rows are marked by white arrows.

The formation of the unidirectional structures demonstrates that the mobility of the molecules at room temperature is sufficient to overcome the diffusion barrier on the surface. On the other hand, the intermolecular interaction strength is large enough to provide stable growth along the molecular row direction. When depositing the molecules onto the calcite substrate held at low temperatures (110 K), individual molecules are observed on the surface (not shown here), indicating that the molecules do not possess sufficient energy to overcome the diffusion barrier at 110 K. This allows for an estimation of a surface diffusion barrier in the range of 0.4 eV < E_d < 1.0 eV.[42] Thus, the observed molecular rows represent a self-assembled structure[43] with the calcite ($10\bar{1}4$) surface acting as a template, as all of the rows align along the [010] direction, exclusively.

In order to gain insights into the mechanism of molecular row formation, we performed high-resolution NC-AFM imaging, which reveals details of the molecular structure. Figure 4 presents a high-resolution image of an individual molecular row. In Figure 4a, the topography channel is shown, whereas Figure 4b represents the corresponding detuning signal. In both channels, an internal structure is clearly resolved. The double-row structure visible in the topography channel (Figure 4a) is formed by pairs of bright features. This is in good agreement with the above assumption; the final molecular rows are composed of molecular pairs. The protrusions within a pair are separated by 11 ± 3 Å, almost perpendicular to the row direction. The periodicity along the row direction can be determined very precisely, as the underlying calcite substrate structure is resolved simultaneously. In Figure 4b, several parallel white lines indicate the double unit cell repeat distance of 2 × 5 Å in the [010] direction, and therefore the periodicity along the double-row structure can unambiguously be identified to 10 Å.

Imaging highly protruding structures with NC-AFM involves numerous problems, including imaging the tip apex,[44] feedback instabilities and entering into the repulsive regime.[45] In Figure 4c and Figure 4d, line profiles taken from the topography (in Figure 4c) and the detuning images (in Figure 4d) are presented, one taken along the row (red) and one perpendicular to the row (black). The same image point is indicated by arrows in all of the subfigures. The corrugation along the molecular row is in the order of 1 Å, whereas the imaged height of the row itself is about ~7 Å with respect to the imaged surface. This height of 7 Å is somewhat smaller than what is expected for an upright standing molecule (about 11.5 Å when taking the van der Waals radii of an individual molecule), indicating that the upright standing molecules might form a tilt angle with respect to the surface normal. This behavior has been observed previously for heptahelicenes on Ni(100),[20] where the helical axis forms an angle of 43 ± 5° with respect to the surface plane. We want, however, to stress explicitly that the measured height represents a plane of identical strength of interaction, namely a plane of equal detuning. Thus, it does not necessarily coincide with the expected height derived from quantum chemical modeling.

Additionally, the appearance of the molecular row is asymmetric, as seen by the black curve in Figure 4c. This asymmetry holds for both the forward and the backward scan lines (not shown). As the molecular structure protrudes from the surface at least by 7 Å compared to the corrugation of the calcite substrate, many atoms of the tip apex can interact with the molecular row. Even for a relatively sharp tip, atoms that are several Ångströms away from the foremost tip atom can, thus, contribute to the measured interaction forces, resulting in the asymmetric appearance, which reflects the asymmetry of the tip apex. The double-row appearance of the molecular structure does, however, represent the true molecular structure. We carefully compared the data taken with a large number of different tips for confirming this point and for explicitly excluding the possibility of a double-tip artifact.

The [7]HCA used in this study consists of a racemic mixture of both (*M*) and (*P*) enantiomers, which are displayed as stick models in Figure 1a. The NC-AFM results indicate an upright standing geometry of the molecules with the helical axis roughly parallel to the [010] direction, but the molecules might be tilted with respect to the surface plane. This interpretation is in agreement with previous results for heptahelicene on Ni(100).[20] Furthermore, two-dimensional islands might be expected in the case of flat-lying [7]HCA (with the helical axis perpendicular to the surface plane as observed for heptahelicene on Cu(111)[18,19] rather than the unidirectional rows of [7]HCA described here.

The upright geometry allows for $\pi-\pi$ stacking of the molecules along the molecular row direction. Moreover, as we observe a transition of less stable single rows to molecular double rows, the molecules within the $\pi-\pi$ stacked row seem to interact with another neighboring row. Considering the molecular structure, it can be readily assumed that the double-row formation is due to the hydrogen bond formation between the carboxylic groups of neighboring [7]HCA molecules.

Possible structural models for such rows composed of molecular pairs are given in the upper part of Figure 5. Owing to molecular chirality, two different kinds of molecular rows can be envisioned, namely homochiral (*M*),(*M*) and (*P*),(*P*) rows, comprising either (*M*) or (*P*) enantiomers exclusively, or heterochiral (*M*),(*P*) rows, containing both enantiomers within the double row. In our NC-AFM images, no differences were observed between the rows, suggesting that heterochiral rows are formed. However, based on the NC-AFM images alone, it is not possible to identify the internal structure clearly, leaving the possibility that existing differences in the case of homochiral double-row formation remain undiscovered, although many high-resolution data of different molecular rows were carefully compared.

In order to obtain basic insights into the organization of [7]HCA on the calcite surface leading to the row formation,

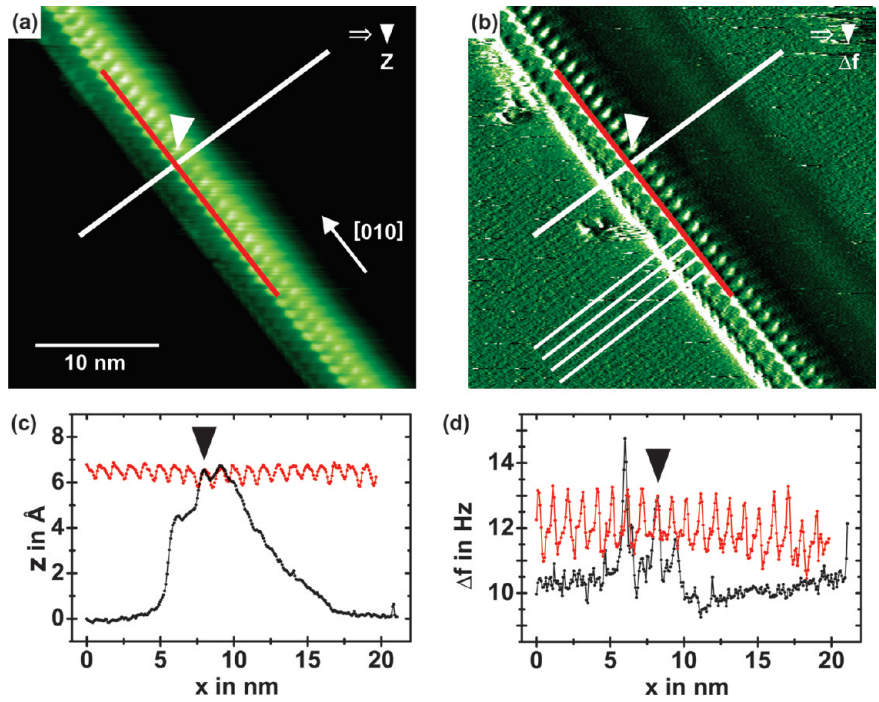

Figure 4. Structure of a paired molecular row as imaged with the NC-AFM in (a) the topography channel and (b) the detuning channel. The same image point is marked in all figures by white and black arrows. (c) Height profiles taken along the indicated lines of (a). (d) Height profiles taken along the indicated lines in (b).

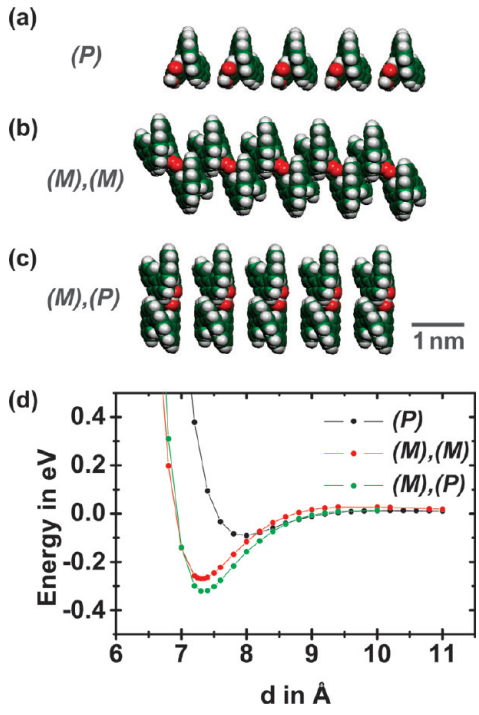

Figure 5. Models for different [7]HCA rows. (a) Single homochiral molecular row. (b) Homochiral molecular double row formed by homochiral molecular pairs. (c) Heterochiral molecular double row formed by heterochiral molecular pairs. (d) Calculated potentials for the above shown different row geometries. (black) Interaction potential of two individual [7]HCA molecules, i.e. forming a single row as shown in (a) (same for (*M*)). (red) Interaction potential of two homochiral pairs, forming a homochiral double row as shown in (b) (same for (*P*),(*P*)). (green) Interaction potential of two heterochiral pairs, forming a heterochiral double row as shown in (c). Note that another arrangement for the heterochiral rows does in principle exist, comprising of homochiral pairs of different chirality. This configuration, however, hampers $\pi-\pi$ stacking and was, thus, omitted in this calculation.

we performed density functional theory (DFT) calculations. As the large size of the surface system with the molecules on top constitutes a challenging task for DFT, we employed several simplifications. All the calculations were performed with the [7]HCA molecules in-vacuo, thus in the absence of the calcite surface.

In the first step, we relaxed the geometry of an individual molecule by minimizing all the forces to less than 0.01 eV/Å. Second, we calculated the interaction potential of two such relaxed molecules in dependence on the molecule−molecule distance, as shown in Figure 5a. Based on this calculation, we obtained a binding energy of about 0.09 eV at an optimum distance of 8 Å for a single row. Furthermore, we calculated the distance-dependent potential for a homo- and a heterochiral molecular double row as shown in Figure 5, panels b and c. For this calculation, we started with two molecules (either homo- or heterochiral) forming hydrogen bonds between the carboxylic groups and relaxed the molecular pair. After obtaining the optimized pair geometry, the distance-dependent potential was calculated by varying the pair−pair distance of two pairs (without further relaxation of the individual pairs). As can be seen, the binding energy is about 0.27 eV per pair for the homochiral double row at an optimum distance of 7.3 Å. For the heterochiral pair we obtain a binding energy of about 0.32 eV and a distance of about 7.3 Å.

The energy difference between the homo- and heterochiral pairs obtained here is too small to be taken literally. This is especially true when considering the simplification made by omitting the substrate surface. Furthermore, DFT calculations do not describe systematically the dispersion forces contributing to the $\pi-\pi$ interactions.[46–50] Fortunately, the local-density approximation (LDA) to the DFT exchange-correlation functional often yields binding energies and distances of weakly interacting objects in reasonable agreement with more elaborate approaches and with experiments.[51–53] Therefore, the calculated data do strongly support the above-drawn conclusion of upright

standing molecules forming rows by $\pi-\pi$ stacking of the aromatic rings. Moreover, the calculations indicate that single molecular rows with a binding energy of only 0.09 eV remain unstable at room temperature, while the formation of heterochiral, molecular double-rows with a binding energy of 0.32 eV seems plausible. This calculated binding energy is relatively small; however, absolute energy values are calculated with rather large error for the reasons discussed above.

Finally, the binding distances obtained from DFT suggest an optimum distance of about 7.3 Å somewhat smaller than the observed periodicity of 10 Å. This difference can be understood by considering a possible tilted alignment of the molecules. Upon tilting the main molecular axis about 43° with respect to the surface plane, the intermolecular distance measured parallel to the helical axes is decreased from initially 10 to 7.3 Å. At the same time, the height of the molecule is reduced from approximately 11.5 to 8.4 Å, which is rather close to the experimentally observed molecular height.

Conclusion

In conclusion, we present the self-assembly of unidirectional molecular structures of racemic [7]HCA on a truly insulating substrate, namely calcite. The molecular rows do not require nucleation sites such as step edges but form on the bare terraces. High-resolution NC-AFM images reveal insights into the molecular geometry, indicating molecular rows formed by upright-standing pairs of [7]HCA molecules with their helical axis tilted with respect to the surface plane. This configuration can be readily understood by $\pi-\pi$ stacking of the molecules within a row and hydrogen bond formation to the neighboring rows. Ab-initio calculations elucidated the detailed geometry and support the assumption of tilted molecules.

This study demonstrates that choosing properly functionalized molecules enables self-assembly of molecular wire-like structures even on insulating surfaces, where high molecular mobility has so far hampered self-assembly of tailor-made molecular structures.

Acknowledgment. Financial support from the Deutsche Forschungsgemeinschaft through the Emmy-Noether grant KU 1980/1-2 is gratefully acknowledged. This research was supported by the European Commission under Grant No. FP6-015847, by the Czech Science Foundation under Grant No. 203/07/1664, by the Ministry of Education, Youth and Sports of the Czech Republic under Project No. LC512 (the Centre for Biomolecules and Complex Molecular Systems) and by the Institute of Organic Chemistry and Biochemistry, Academy of Sciences of the Czech Republic (this work is part of the Research Project Z4 055 0506). We thank the group of Prof. Marek Szymonski for most useful information regarding the helicene sublimation.

References and Notes

(1) Moore, G. E. *Electronics* **1965**, *38*, 114–116.
(2) Joachim, C.; Gimzewski, J. K.; Aviram, A. *Nature* **2000**, *408*, 541–548.
(3) Joachim, C.; Gimzewski, J. K.; Tang, H. *Phys. Rev. B* **1998**, *58* (24), 16407–16417.
(4) Maier, S.; Fendt, L.-A.; Zimmerli, L.; Glatzel, T.; Pfeiffer, O.; Diederich, F.; Meyer, E. *Small* **2008**, *4* (8), 1115–1118.
(5) Tans, S. J.; Verschueren, A. R. M.; Dekker, C. *Nature (London)* **1998**, *393* (6680), 49–52.
(6) Barth, J. V. *Ann. Rev. Phys. Chem.* **2007**, *58*, 375–407.
(7) Kühnle, A. *Curr. Opin. Colloid Interface Sci.* **2009**, *14*, 157–168.
(8) Böhringer, M.; Morgenstern, K.; Schneider, W.-D.; Berndt, R.; Mauri, F.; Vita, A. D.; Car, R. *Phys. Rev. Lett.* **1999**, *83*, 324–327.
(9) Pawin, G.; Wong, K. L.; Kwon, K. Y.; Bartels, L. *Science* **2006**, *313* (5789), 961–962.
(10) Theobald, J. A.; Oxtoby, N. S.; Phillips, M. A.; Champness, N. R.; Beton, P. H. *Nature (London)* **2003**, *424* (6952), 1029–1031.
(11) Glatzel, T.; Zimmerli, L.; Koch, S.; Kawai, S.; Meyer, E. *Appl. Phys. Lett.* **2009**, *94* (6), 063303.
(12) Kawai, S.; Maier, S.; Glatzel, T.; Koch, S.; Such, B.; Zimmerli, L.; Fendt, L. A.; Diederich, F.; Meyer, E. *Appl. Phys. Lett.* **2009**, *95* (10), 103109.
(13) Nony, L.; Bennewitz, R.; Pfeiffer, O.; Gnecco, E.; Baratoff, A.; Meyer, E.; Eguchi, T.; Gourdon, A.; Joachim, C. *Nanotechnology* **2004**, *15* (2), S91.
(14) Kunstmann, T.; Schlarb, A.; Fendrich, M.; Wagner, T.; Möller, R.; Hoffmann, R. *Phys. Rev. B* **2005**, *71* (12), 121403.
(15) Fendrich, M.; Kunstmann, T. *Appl. Phys. Lett.* **2007**, *91* (2), 023101−3.
(16) Treboux, G.; Lapstun, P.; Wu, Z. H.; Silverbrook, K. *Chem. Phys. Lett.* **1999**, *301* (5−6), 493–497.
(17) Ernst, K. H.; Kuster, Y.; Fasel, R.; Muller, M.; Ellerbeck, U. *Chirality* **2001**, *13* (10), 675–678.
(18) Fasel, R.; Cossy, A.; Ernst, K. H.; Baumberger, F.; Greber, T.; Osterwalder, J. *J. Chem. Phys.* **2001**, *115* (2), 1020–1027.
(19) Fasel, R.; Parschau, M.; Ernst, K.-H. *Nature (London)* **2006**, *439* (7075), 449–452.
(20) Ernst, K. H.; Neuber, M.; Grunze, M.; Ellerbeck, U. *J. Am. Chem. Soc.* **2001**, *123* (3), 493–495.
(21) Ernst, K.-H.; Böhringer, M.; McFadden, C. F.; Hug, P.; Müller, U.; Ellerbeck, U. *Nanotechnology* **1999**, *10*, 355–361.
(22) Addadi, L.; Weiner, S. *Angew. Chem.-Int. Ed. Engl.* **1992**, *31* (2), 153–169.
(23) Addadi, L.; Weiner, S. *Nature* **2001**, *411*, 753–755.
(24) Kristensen, R.; Stipp, S. L. S.; Refson, K. *J. Chem. Phys.* **2004**, *121* (17), 8511–8523.
(25) Giessibl, F. J. *Rev. Mod. Phys.* **2003**, *75* (3), 949–983.
(26) Schütte, J.; Rane, P.; Tröger, L.; Rode, S.; Bechstein, R.; Reichling, M.; Kühnle, A. **2009**, submitted.
(27) Tröger, L.; Schütte, J.; Ostendorf, F.; Kühnle, A.; Reichling, M. *Rev. Sci. Instrum.* **2009**, *80* (6), 063703.
(28) Hassine, B. B.; Gorsane, M.; Pecher, J.; Martin, R. H.; Defay, N.; Ottinger, R. *Bull. Soc. Chim. Belges* **1985**, *94* (6), 425–430.
(29) Teplý, F.; Stará, I. G.; Starý, I.; Kollárovič, A.; Šaman, D.; Rulíšek, L.; Fiedler, P. *J. Am. Chem. Soc.* **2002**, *124* (31), 9175–9180.
(30) Teplý, F.; Stará, I. G.; Starý, I.; Kollárovič, A.; Šaman, D.; S., V.; Fiedler, P. *J. Org. Chem.* **2003**, *68* (13), 5193–5197.
(31) Alexandrová, Z.; Sehnal, P.; Stará, I. G.; Starý, I.; Šaman, D.; Urquhart, S. G.; Otero, E. *Collect. Czech. Chem. Commun.* **2006**, *71*, 1256–1264.
(32) Míšek, J.; Teplý, F.; Stará, I. G.; Tichý, M.; Šaman, D.; Císařová, I.; Vojtíšek, P.; Starý, I. *Angew. Chem., Int. Ed.* **2008**, *47* (17), 3188–3191.
(33) Schütte, J.; Bechstein, R.; Rahe, P.; Rohlfing, M.; Langhals, H.; Kühnle, A. *Phys. Rev. B* **2009**, *79* (4), 045428.
(34) Albrecht, T. R.; Grütter, P.; Horne, D.; Rugar, D. *J. Appl. Phys.* **1991**, *69* (2), 668–673.
(35) Ceperley, D. M.; Alder, B. J. *Phys. Rev. Lett.* **1980**, *45* (7), 566–569.
(36) Ordejon, P.; Artacho, E.; Soler, J. M. *Phys. Rev. B* **1996**, *53* (16), 10441–10444.
(37) Soler, J. M.; Artacho, E.; Gale, J. D.; Garcia, A.; Junquera, J.; Ordejon, P.; Sanchez-Portal, D. *J. Phys.: Condensed Matter* **2002**, *14* (11), 2745–2779.
(38) Troullier, N.; Martins, J. L. *Phys. Rev. B* **1991**, *43* (3), 1993–2006.
(39) Ostlund, N. S.; Merrifield, D. L. *Chem. Phys. Lett.* **1976**, *39* (3), 612–614.
(40) Boys, S. F.; Bernardi, F. *Mol. Phys.* **1970**, *19* (4), 553–&.
(41) At coverages of 1 ML, a closed film exhibiting a (2 × 3) superstructure is observed. In each supercell, two [7]HCA molecules are present and, consequently, one molecule occupies an area of 1.215 nm^2 on the calcite surface.
(42) These energy values are obtained by considering the onset of hopping with a hopping frequency of 10^{-5} s^{-1} and an attempt frequency of 10^{12} s^{-1}.
(43) Whitesides, G. M.; Mathias, J. P.; Seto, C. T. *Science (Washington, DC)* **1991**, *254* (5036), 1312–19.
(44) Pakarinen, O. H.; Barth, C.; Foster, A. S.; Henry, C. R. *J. Appl. Phys.* **2008**, *103* (5), 054313.
(45) Rahe, P.; Bechstein, R.; Schütte, J.; Ostendorf, F.; Kühnle, A. *Phys. Rev. B* **2008**, *77* (19), 195410.

(46) Grimme, S. *J. Comput. Chem.* **2004**, *25* (12), 1463–1473.
(47) Grimme, S. *J. Comput. Chem.* **2006**, *27* (15), 1787–1799.
(48) Valdes, H.; Klusak, V.; Pitonak, M.; Exner, O.; Starý, I.; Hobza, P.; Rulisek, L. *J. Comput. Chem.* **2008**, *29* (6), 861–870.
(49) Rulíšek, L.; Exner, O.; Cwiklik, L.; Jungwirth, P.; Starý, I.; Pospíšil, L.; Havlas, Z. *J. Phys. Chem. C* **2007**, *111*, 14948–14955.
(50) Sehnal, P.; Stará, I. G.; Šaman, D.; Tichý, M.; Míšk, J.; Cvačka, J.; Rulíšek, L.; Chocholoušová, J.; Vacek, J.; Goryl, G.; Szymonski, M.; Císařová, I.; Starý, I. *Proc. Natl. Acad. Sci.* **2009**.
(51) Marini, A.; Garcia-Gonzalez, P.; Rubio, A. *Phys. Rev. Lett.* **2006**, *96* (13), 136404.
(52) Harl, J.; Kresse, G. *Phys. Rev. B* **2008**, *77* (4), 045136.
(53) Rohlfing, M.; Bredow, T. *Phys. Rev. Lett.* **2008**, *101* (26), 266106.

JP911287P